JOURNAL OF CATALYSIS **169,** 1–12 (1997)
ARTICLE NO. CA971670

Heterogeneous Coupling of Phenylethyne over Cu–Mg–Al Mixed Oxides

Influence of Catalyst Composition and Calcination Temperature on Structural and Catalytic Properties

S. M. Auer, R. Wandeler, U. Göbel, and A. Baiker[1]

Department of Chemical Engineering and Industrial Chemistry, Swiss Federal Institute of Technology, ETH Zentrum, CH-8092 Zürich, Switzerland

Received June 28, 1996; revised November 18, 1996; accepted January 7, 1997

Cu–Mg–Al mixed oxides in basic media are shown to be efficient catalysts in the oxidative coupling of phenylethyne to 1,4-diphenylbuta-1,3-diyne. Catalysts containing 33 at.% of Cu(II), related to the total metal content, with different ratios of Mg(II) and Al(III) were prepared by precipitation of metal nitrates with sodium carbonate and calcined at different temperatures. The samples were characterized by means of XRD, TEM, TG-MS, XPS, N_2O titration, and N_2 physisorption. The catalytic behavior was tested in *n*-butanol (0–0.1 *M* NaOH) in an autoclave under oxygen atmosphere (0.5–4 MPa) at different temperatures (303–353 K). Highest yields of 1,4-diphenylbuta-1,3-diyne (84%) were obtained with catalysts based on Cu–Mg–Al lamellar double hydroxides (LDHs). Typical selectivities to 1,4-diphenylbuta-1,3-diyne were in the range of 85–92%, depending on reaction conditions and conversion. Cu(II) on the catalyst surface was found to be crucial as a redox site in the coupling of phenylethyne. However, the mere presence of Cu(II) on the surface is not sufficient for a highly active catalyst. Cu(II) must be embedded into a specific matrix in order to exhibit high catalytic activity. The hydrotalcite-like phase (LDH) in Cu–Mg–Al catalysts provides such a matrix.

INTRODUCTION

Lamellar double hydroxides (LDHs) consist of positively charged metal hydroxide layers separated from each other by anions and water molecules. The layers contain metal ions of at least two different oxidation states. The most common case of di- and trivalent cations leads to the general chemical formula $[M(II)_{1-x}M(III)_x(OH)_2]^{x+}(A^{n-})_{x/n} \cdot mH_2O$, where x refers to the $n[M(III)]/n[M(II)+M(III)]$ ratio ranging between ca. 0.25 and 0.4 (1). The positive charge of the metal hydroxide layers is compensated by interstitial layers built of anions A^{n-} and crystal water. LDHs are also referred to as anionic clays (2–4), double hydroxides (5, 6), hydrotalcite-like compounds (7–9), or pillared hydroxycarbonates (10). De Roy *et al.* (11) have reviewed LDHs concentrating on preparation, structure, ion exchange, and pillaring.

In a comprehensive review Cavani *et al.* (1) discuss the structural and catalytic properties of LDHs. In catalysis, LDHs are either used as such or, more often, after calcination. Calcined LDHs form highly dispersed mixed oxides stable to thermal treatments. They possess basic and redox properties, depending on the metal cations built into the layered matrices. In basic catalysis, LDHs are applied in polymerization of alkene oxides (12, 13), aldol condensations (14), and other reactions. In redox catalysis, they are used as mixed oxide catalysts in gas-phase reactions such as methanol synthesis (15) and a few fine chemical reactions, e.g., Baeyer–Villiger oxidation with oxygen and benzaldehyde (16).

In order to investigate the catalytic properties of LDHs, we focused on a catalytic reaction which involves both basic and redox elementary steps and is catalyzed by uncalcined as well as calcined LDHs. In a preliminary study (17) we have shown that the oxidative coupling of phenylethyne to 1,4-diphenylbuta-1,3-diyne catalyzed by a Cu–Mg–Al LDH and sodium hydroxide fulfills these requirements (Scheme 1). Sodium hydroxide must be used as a cocatalyst since the intrinsic basicity of the LDH does not suffice for the deprotonation step of the coupling reaction. Modification of the reactant leads to substituted 1,4-diphenylbuta-1,3-diynes which form an important class of liquid crystals for use in infrared and long wavelength application (18). Note that previous to our studies only the homogeneously catalyzed coupling of phenylethyne has been reported (19, 20).

The aim of this study was to elucidate the relation between structural and chemical properties of different Cu–Mg–Al LDHs and mixed oxides and their catalytic behavior in the coupling of phenylethyne.

[1] To whom correspondence should be addressed. Fax: +41 1 632 11 63. E-mail: a.baiker@tech.chem.ethz.ch.

0021-9517/97 $25.00

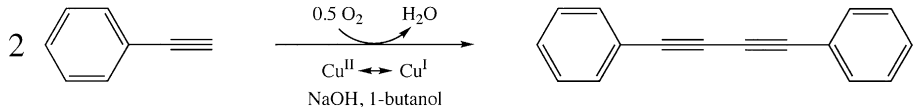

SCHEME 1. Reaction scheme of the Cu-catalyzed oxidative coupling of phenylethyne.

EXPERIMENTAL

Preparation

Various amounts of $Cu(NO_3)_2 \cdot 3H_2O$, $Mg(NO_3)_2 \cdot 6H_2O$, and $Al(NO_3)_3 \cdot 9H_2O$ (total metal nitrates, 0.24 mol) were dissolved in 500 ml distilled water and transferred into a 1l five-necked flask equipped with propeller mixer, reflux condenser, pH meter (Metrohm 614 pH meter), thermocouple, and feeding unit for liquids. This system was equilibrated at 333 ± 2 K under vigorous stirring. Subsequently, 300 to 500 ml 0.75 *M* Na_2CO_3 solution was slowly added (Metrohm 665 Dosimat) to the metal nitrate solution over a time period of 2 h until a pH of 8 was reached. The light-blue suspension was stirred for 15 h at room temperature and filtered. The precipitates were intensively washed with distilled water and dried at 363 K below 10 kPa for 24 h. The obtained samples were calcined for 4 h at 15 Pa and different temperatures.

Preliminary tests using other preparation methods like precipitation at low or high supersaturation according to (1) led to catalysts with lower activity in the phenylethyne coupling reaction.

Characterization

Catalyst materials were investigated with regard to their physical and chemical properties by means of powder X-ray diffraction (XRD), transmission electron microscopy (TEM), thermoanalytical analysis (TG, DTA) in combination with mass spectrometry (MS), X-ray photoelectron spectroscopy (XPS), nitrous oxide titration, and nitrogen physisorption.

X-ray diffraction patterns were measured on a Siemens D5000 powder X-ray diffractometer. Diffractograms were recorded with detector-sided Ni-filtered Cu$K\alpha$ radiation (40 mA, 40 kV) over a 2θ-range of 2° to 70° and a position sensitive detector using a step size of 0.010° and a step time of 2.5 s. Measured patterns were compared with JCPDS data files (21). Mean crystallite sizes were estimated using the Scherrer equation (22, 23) and the widths of selected diffraction lines which were fitted with a Split Pearson 7 function. Peak broadening due to the instrumental line broadening of $2\theta = 0.08^\circ$ was taken into account (24).

Transmission electron microscopy was carried out using a Philips CM30ST electron microscope with a CeB_6-cathode and an acceleration voltage of 300 kV.

Thermoanalytical measurements (TG, DTA) were performed on a Netzsch STA 409 using α-Al_2O_3 as a reference and a heating rate of 10 K min^{-1} in the temperature range of 298 to 1323 K. Evolving gases were monitored on-line using a Balzers QMG 420 quadrupole mass spectrometer connected to the thermoanalyzer by a heated capillary.

XPS analyses were performed on a Leybold LHS 11 instrument with Mg$K\alpha$ radiation (240 W). The analyzer was operated at 150 eV constant pass energy at a scale calibrated versus the Au4$f^{7/2}$ line at 84.0 eV. Corrections of the energy shift, due to the steady-state charging effect, were accomplished taking the C1*s* line of adsorbed hydrocarbons at 285.0 eV as internal standard. Samples were degassed at 2×10^{-9} mbar for 3 days before analysis. For an estimation of the surface composition in mol%, the intensities of the elemental peaks Na1*s*, C1*s*, O1*s*, Cu2$p^{3/2}$, Mg2*p*, and Al2*s* were determined by a curve-fitting program (25) and divided by the corresponding atomic sensitivity factors (26).

Cu surface areas were determined by N_2O titration using a pulse technique similar to that reported by Evans *et al.* (27). H_2 and He were of ultra high purity. He was further freed from O_2 using an Oxisorb system (Messer Griessheim). N_2O (Matheson, 99.998%) was dried over a column filled with activated molecular sieve, type 4 Å. Samples were reduced in flowing H_2/Ar (5% hydrogen, 75 cm^3 min^{-1}) by heating from 373 to 548 K at 5 K min^{-1}. The samples were held at this temperature for 15 min and then exposed to pure H_2 (75 cm^3 min^{-1}) for 30 min at the same temperature. The H_2 was purged with He (50 cm^3 min^{-1}) at 548 K. After cooling to 363 K under He, pulses of N_2O (0.5 cm^3) were injected. N_2 and N_2O were separated on a Porapak N column and detected by means of a thermal conductivity detector (Gow Mac Instruments). Cu metal surface areas were calculated assuming 1.46×10^{19} Cu atoms/m^2 (27, 28) and an adsorption stoichiometry of $Cu_{(s)}/O_{(ads)} = 2$. The accuracy of the copper surface area measurements was within 5%.

BET surface areas (S_{BET}), mean cylindrical pore diameters ($\langle d_p \rangle$) and specific adsorption pore volumes (V_{p,N_2}) were obtained by physisorption of nitrogen at 77 K using a Micromeritics ASAP 2000 instrument. Prior to measurement, the samples were degassed to 0.1 Pa at 473 K. S_{BET} were calculated in a relative pressure range between $0.05 < p/p_0 < 0.2$ assuming a cross-sectional area of 0.162 nm^2 for the nitrogen molecule. Pore size distributions were calculated applying the Barrett–Joyner–Halenda (BJH) method (29) to the desorption branch of the isotherms (30). The assessments of microporosity were made from *t*-plot constructions ($0.3 < t < 0.5$ nm) using the Harkins–Jura correlation (31).

Catalytic Tests

Coupling of phenylethyne was carried out in a 100-ml stainless-steel autoclave (Baskerville R&A) equipped with a 50-ml glass liner and a PTFE lid. The reaction mixture was stirred with a magnetic PTFE stirrer (0–1500 rpm). The reactor was heated by a 10 l heating bath ($\Delta T = \pm 2$ K) connected to a temperature controlling unit. Preliminary tests showed that a constant temperature of the reaction mixture was reached after 30-min equilibration time at 100 rpm. Oxygen pressure in the reactor was maintained using a gas dosing unit with reducing valve (Tescom) compensating for O_2 consumed during the reaction.

The reaction mixture comprised 2 g phenylethyne (Fluka 98%, 2% styrene), 50 mg catalyst ($\leq$180 μm particle size), and different amounts of dry NaOH dissolved in 25 ml 1-butanol (0–0.1 *M* NaOH). In order to equilibrate the system, the reaction mixture was kept under N_2 (99.998%) at the desired reaction temperature for 30 min at 100 rpm. The starting procedure, which lasted about 15 s, involved purging of the autoclave with O_2 (99.998%) and adjusting the desired oxygen pressure (0.5–4 MPa) and stirring speed (1000 rpm). At the end of the reaction, the pressure was released and the stirrer was stopped. Catalytic tests quoted in this article were performed over a time period of 15 min.

Phenylethyne conversion and selectivity to 1,4-diphenylbuta-1,3-diyne were determined by GC analysis (HP1, FID) using pentadecane (Fluka) as internal standard. Conversions and selectivities were reproducible within ± 2 and ± 5%, respectively.

The reaction mixtures were analyzed for dissolved Cu species by AAS using a Varian SpectrAA-10BQ atomic absorption spectrometer. After filtration through a 0.2-μm PTFE filter (Infochroma), the reaction samples were mixed with 0.1 *M* HNO_3 in water and washed with diethylether to suppress matrix effects of organics during measurement. The aqueous phase was concentrated in a rotary evaporator and analyzed using a Varian AA copper lamp (4 mA, slit 0.5, 324.8 nm).

RESULTS

All catalysts prepared, LDHs and mixed oxides, were based on Cu(II) as well as Mg(II) and/or Al(III). The samples contained 33 at.% of Cu(II) related to the total metal content, affording catalysts of type $[Cu_{0.33}Mg_{(0.67-x)}-Al_x-CO_3]$ according to the denotation suggested by De Roy *et al.* (11). The *x* value of the samples, i.e., the ratio of Al(III) to total metal content, was varied between 0.67 and 0.0. The composition of our catalysts is fully defined by the *x* value. We will therefore use the denotation $[Cu\text{-}x]_T$ for our samples, where *T* is the calcination temperature of the compound in K. Uncalcined catalysts are indicated by the subscripts uc. The compositions of the investigated Cu–Mg–Al mixed oxides ($[Cu\text{-}0.67]_T$, $[Cu\text{-}0.33]_T$, $[Cu\text{-}0.29]_T$, $[Cu\text{-}0.25]_T$, $[Cu\text{-}0.0]_T$), are depicted in Fig. 1 as a function of both n[Cu(II)]/n[M(II)] and *x* value.

Characteristic Features of Phenylethyne Coupling Reaction

The influence of the reaction parameters on the phenylethyne coupling reaction (Scheme 1) was investigated using $[Cu\text{-}0.33]_{673}$. Conversion of phenylethyne and selectivity to 1,4-diphenylbuta-1,3-diyne depended on sodium hydroxide concentration (0–0.1 *M*), oxygen pressure (0.5–4 MPa), and reaction temperature (303–353 K) as shown in Table 1. Conversion of phenylethyne increased when these three reaction parameters were increased in the given ranges. In contrast, selectivity decreased with increasing sodium hydroxide concentration and reaction temperature. Without sodium hydroxide, no conversion was observed. Preliminary optimization of the reaction conditions ($[Cu\text{-}0.33]_{673}$, 0.1 *M* NaOH, 2 MPa O_2, 353 K) led to 84% yield of 1,4-diphenylbuta-1,3-diyne (Table 1).

The reaction rate was independent on stirring speed ($>$750 rpm) and catalyst particle size ($<$315 μm) indicating that the reaction rate was not influenced by interparticle or intraparticle mass transfer limitations in the chosen parameter range. In addition, the reaction rate was linearly dependent on the amount of catalyst below amounts of 100 mg, implying that transfer of oxygen from gas to liquid phase did not limit the observed reaction rate.

Side products were determined in the reaction using 0.1 *M* NaOH solution and 2 MPa oxygen pressure at 333 K. At low conversion, butyl phenylacetate was produced in a homogeneous side reaction consuming ca. 5% of phenylethyne converted. At higher conversions no side products were detected by GC/MS, possibly due to polymerization or complete oxidation of butyl phenylacetate;

TABLE 1

Dependence of Conversion of Phenylethyne and Selectivity to 1,4-Diphenylbuta-1,3-diyne on NaOH Concentration, O_2 Pressure, and Reaction Temperature

c(NaOH) (*M*)	O_2 pressure (MPa)	Reaction temperature (K)	Conversion (%)	Selectivity (%)
0.1	2	333	74	86
0.075	2	333	47	88
0.05	2	333	32	92
0.1	4	333	84	87
0.1	1	333	26	85
0.1	0.5	333	14	70
0.1	2	353	97	87
0.1	2	323	16	94
0.1	2	313	5	99
0.1	2	303	1	—

Note. Reactions were performed with $[Cu\text{-}0.33]_{673}$ (calcined at 673 K) for 15 min. Note that no reaction was observed in the absence of the catalyst.

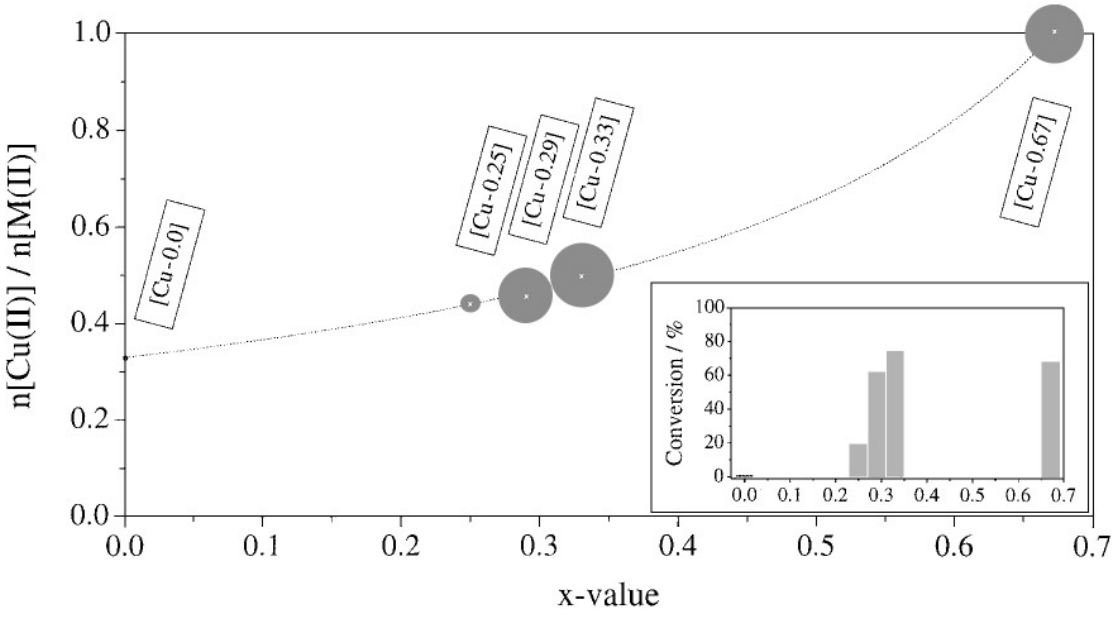

FIG. 1. Influence of catalyst composition on conversion of phenylethyne. Bulk composition of the Cu–Mg–Al mixed oxides is depicted as a function of both n[Cu(II)]/n[M(II)] and x value ($x = n$[M(III)]/n[M(II) + M(III)]). Conversion of phenylethyne is proportional to the bubble diameter at the corresponding catalyst composition. The dotted line represents catalyst compositions with a Cu(II) content of 33 at.% related to total metal content. Phenylethyne conversion is additionally shown in a bar graph as a function of x value only. Reactions were performed in 0.1 *M* NaOH at 2 MPa O_2 pressure and 333 K for 15 min; catalysts were calcined at 673 K. [Cu-x], catalyst with a Cu(II) content of 33 at.% related to total metal content and the indicated x value; n[Cu(II)], molar amount of Cu(II); n[M(II)], molar amount of divalent metal; n[M(III)], molar amount of trivalent metal; n[M(II) + M(III)], total molar amount of di- and trivalent metal.

however, neither the polymer nor the possible side product CO_2 could be detected. Moreover, about 0.2 mg of yellow copper(I)phenylethynilide (32) was formed, as evidenced by XRD. This compound exhibited some catalytic activity in the coupling reaction, contributing ca. 1% to the overall conversion of phenylethyne.

The amount of copper dissolved in the reaction medium depended significantly on the sodium hydroxide concentration. Up to ca. 0.15 *M* sodium hydroxide, the concentration of dissolved copper remained below the resolution limit of AAS ($<5 \times 10^{-4}$ *M* Cu); higher sodium hydroxide concentrations led to an increase in the formation of soluble copper hydroxide species (1.5×10^{-3} *M* dissolved copper in 0.4 *M* NaOH). In contrast to copper(I)phenylethynilide, the amount of copper dissolved at sodium hydroxide concentrations below 0.15 *M* did not result in a detectable contribution to catalytic activity.

Catalyst Properties

Influence of composition. The catalytic activity in the coupling of phenylethyne in relation to the bulk composition of the Cu–Mg–Al mixed oxides is shown in Fig. 1. For constant Cu content, conversion generally increased with increasing x value, except for $[\text{Cu-0.67}]_{673}$ which was slightly less active than $[\text{Cu-0.33}]_{673}$. Interestingly, selectivity to 1,4-diphenylbuta-1,3-diyne was almost independent on catalyst composition (Table 3).

Crystalline phases of the samples after precipitation, calcination, and reaction were determined by XRD (Fig. 2). After precipitation (Fig. 2a), two crystalline phases were detected, a hydrotalcite-like phase (HT-phase; JCPDS 37-0630) and a magnesium-copper hydroxide nitrate phase (MgCu-phase; JCPDS 26-1221, 15-0014) (21). With increasing x value, the content of crystalline HT-phase increased, whereas the content of crystalline MgCu-phase decreased. In $[\text{Cu-0.25}]_{uc}$ and $[\text{Cu-0.29}]_{uc}$ both phases coexisted, whereas $[\text{Cu-0.0}]_{uc}$ and $[\text{Cu-0.33}]_{uc}$ showed exclusively reflections of one phase, MgCu or HT respectively. The pattern of $[\text{Cu-0.67}]_{uc}$ only exhibited weak reflections similar to the HT-phase. After calcination at 673 K (Fig. 2b), all samples contained crystalline CuO (JCPDS 41-0254) (21). Crystallinity of this phase decreased with increasing x value (crystallite size data in Table 2). In addition to CuO, $[\text{Cu-0.0}]_{673}$ contained crystalline MgO (JCPDS 4-0829) (21). After reaction (Fig. 2c), all samples showed similar patterns to those before reaction. $[\text{Cu-0.67}]_{673}$, $[\text{Cu-0.33}]_{673}$, and $[\text{Cu-0.29}]_{673}$ contained crystalline Cu-phenylethynilide (32) after reaction. In $[\text{Cu-0.0}]_{673}$ crystalline $Mg(OH)_2$ (JCPDS 44-1482) (21) was detected after reaction instead of MgO present before reaction.

Surface areas, pore volumes, and mean pore diameters did not exhibit a singular trend (Table 2). However, graphically assessed maxima of the pore size distributions were similar for all samples, except for $[\text{Cu-0.67}]_{673}$, which

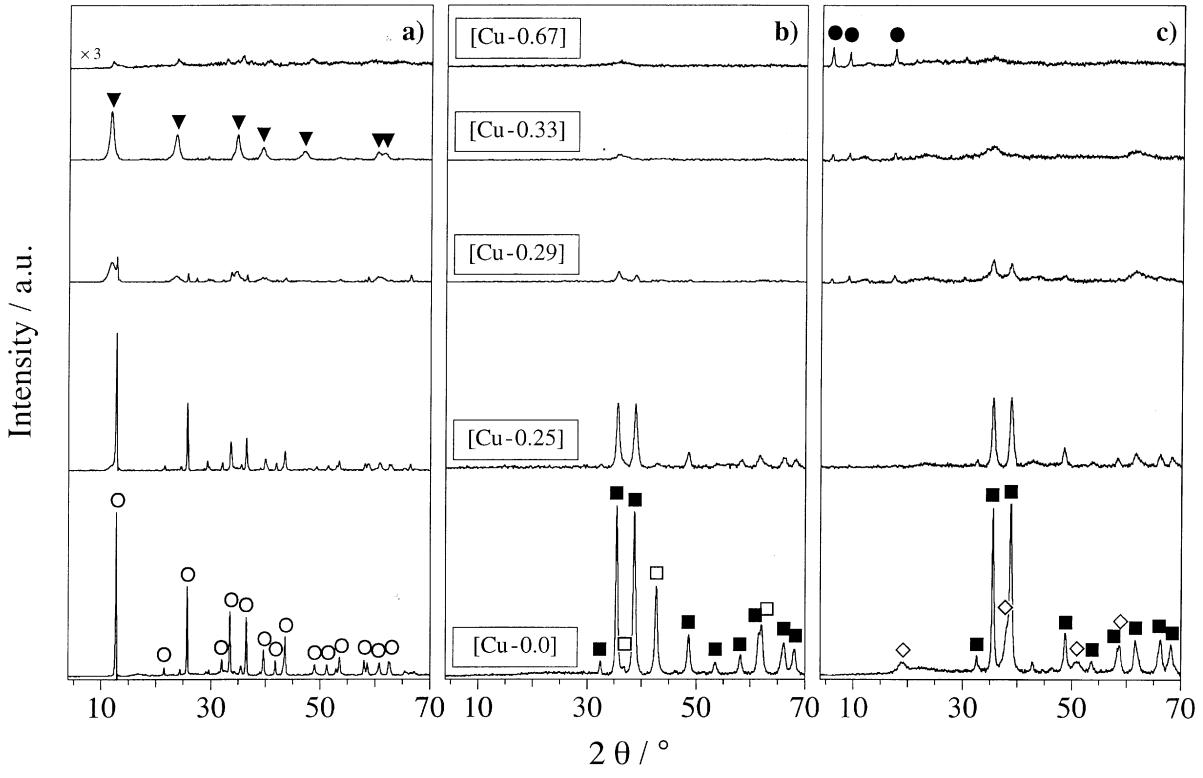

FIG. 2. X-ray diffraction pattern of [Cu-0.0], [Cu-0.25], [Cu-0.29], [Cu-0.33], and [Cu-0.67]. (▼) Hydrotalcite-like phase (HT-phase); (◯) Cu–Mg hydroxide nitrate (MgCu-phase); (■) CuO; (□) MgO; (◇) $Mg(OH)_2$; (●) Cu(I)phenylethynilide. (a) uncalcined; (b) calcined at 673 K; (c) after reaction.

showed a bimodal pore size distribution with an additional microporous maximum. All isotherms were of type-IV with a type-H3 hysteresis according to IUPAC (33), which is generally observed for mesoporous aggregates of plate-like particles. Since all samples exhibited similar morphology, intraparticle mass transfer was expected to be similar to that in $[Cu\text{-}0.33]_{673}$ for all catalysts.

Gases evolved by thermal decomposition of the uncalcined samples during thermoanalytical measurements were monitored by MS (Fig. 3). The binary samples [Cu-0.0] and [Cu-0.67] exhibited a different thermal behavior than the ternary compounds, as expected from the major differences in composition. The decomposition pattern of [Cu-0.29] contained characteristic features of both [Cu-0.25] and [Cu-0.33].

Cu surface areas of samples calcined at 673 K, determined by N_2O titration and corroborated by XPS are listed in Table 3. The ternary samples all exhibited higher Cu surface areas than $[Cu\text{-}0.0]_{673}$ and $[Cu\text{-}0.67]_{673}$. After reaction, the catalysts showed smaller Cu surface areas in N_2O titration than after calcination, most likely due to deposition of organic residues on the catalyst surface (during reaction), which could not be removed completely during pretreatment prior to N_2O titration.

TABLE 2

Morphological Properties of Catalysts $[Cu\text{-}x]_{673}$ (Calcined at 673 K) Determined by N_2 Physisorption and XRD

Bulk composition x value	S_{BET}[a] ($m^2\ g^{-1}$)	V_{p,N_2}[b] ($cm^3\ g^{-1}$)	$d_{p,max}$ ($\langle d_p \rangle$)[c] (nm)	Crystallite size[d] CuO (nm)
0.67	131	0.13	3, 20 (5)	<3
0.33	72	0.52	30 (29)	3
0.29	55	0.38	35 (28)	10
0.25	73	0.41	30 (22)	15
0.0	36	0.29	35 (30)	20

[a] BET surface area.
[b] BJH cumulative desorption pore volume.
[c] Graphically assessed maximum of pore size distribution (in parentheses: mean pore diameter, $\langle d_p \rangle = 4V_{p,N_2}/S_{BET}$).
[d] Determined from XRD line broadening.

Influence of calcination temperature. The influence of calcination temperature on structure and catalytic activity in the coupling of phenylethyne was investigated for the most active catalyst [Cu-0.33].

Catalytic activity in relation to calcination temperature is listed in Table 4. Up to a calcination temperature of 773 K, high conversions were obtained. Calcination at 873 K led to a prominent loss of catalytic activity. Interestingly, selectivity to 1,4-diphenylbuta-1,3-diyne did not depend significantly on calcination temperature.

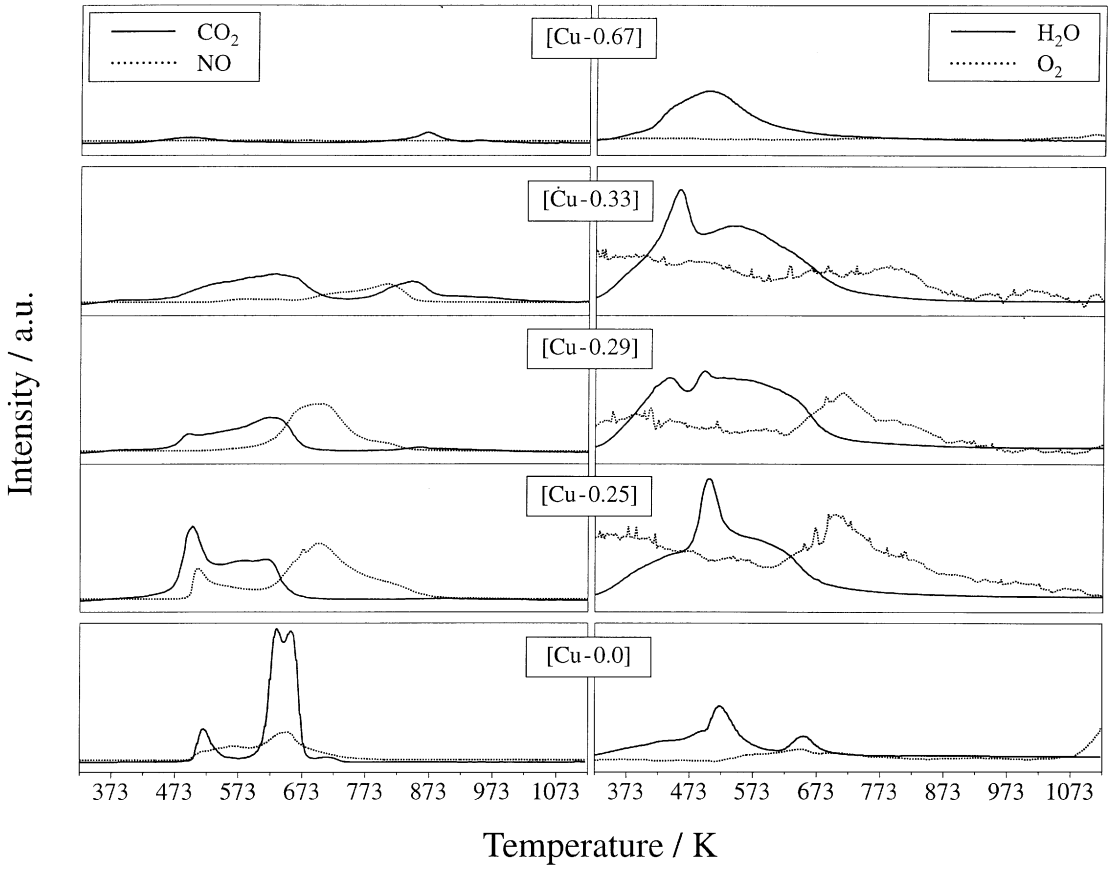

FIG. 3. Evolving gases during thermal decomposition of [Cu-0.0], [Cu-0.25], [Cu-0.29], [Cu-0.33], and [Cu-0.67] as monitored by MS.

Crystalline phases of the sample after calcination at different temperatures were determined by XRD (Fig. 4). $[Cu\text{-}0.33]_{uc}$ showed the diffraction pattern of hydrotalcite-like phases (JCPDS 37-0630) (21). With increasing calcination temperature, crystallinity of this phase declined, leading to a predominantly amorphous catalyst after calcination at 673 K. With higher calcination temperatures, crystalline CuO (JCPDS 41-0254), MgO (JCPDS 4-0829), and $CuAl_2O_4$ (JCPDS 33-0448) phases were formed (21). This behavior is in accordance with the literature (3). Mean crystallite sizes of HT and CuO for different calcination temperatures are listed in Table 5.

TABLE 3

Cu Surface Area Measured by XPS and N_2O Titration, Conversion to Phenylethyne, and Selectivity to 1,4-Diphenylbuta-1,3-diyne for Catalysts $[Cu\text{-}x]_{673}$ (Calcined at 673 K)

Bulk composition *x* value	Cu surface area: N_2O titration ($m^2\ g^{-1}$)[a]	Cu surface area: XPS (%)[b]	Conversion (%)	Selectivity (%)
0.67	3 (2)	—	68	86
0.33	8 (4)	10 {7}	74	86
0.29	9 (6)	8 {5}	62	87
0.25	6 (5)	4 {3}	19	90
0.0	2 (1)	—	1	—

[a] In parentheses: results after reaction.

[b] Values in curled brackets represent Cu surface areas ($m^2\ g^{-1}$) estimated by multiplication of XPS-derived Cu surface concentrations (%) with corresponding BET surface areas ($m^2\ g^{-1}$).

TABLE 4

Cu Surface Area Measured by XPS and N_2O Titration, Conversion to Phenylethyne, and Selectivity to 1,4-Diphenylbuta-1,3-diyne for [Cu-0.33] Calcined at Different Temperatures

Calcination temperature (K)	Cu surface area: N_2O titration ($m^2\ g^{-1}$)	Cu surface area: XPS (%)[a]	Conversion (%)	Selectivity (%)
Uncalcined	4	6 {4}	78	89
473	5	7 {5}	82	89
573	7	10 {7}	66	86
673	8	10 {7}	74	86
773	12	10 {7}	78	88
873	10	8 {6}	28	86

[a] Values in curled brackets represent Cu surface areas ($m^2\ g^{-1}$) estimated by multiplication of XPS-derived Cu surface concentrations (%) with corresponding BET surface areas ($m^2\ g^{-1}$).

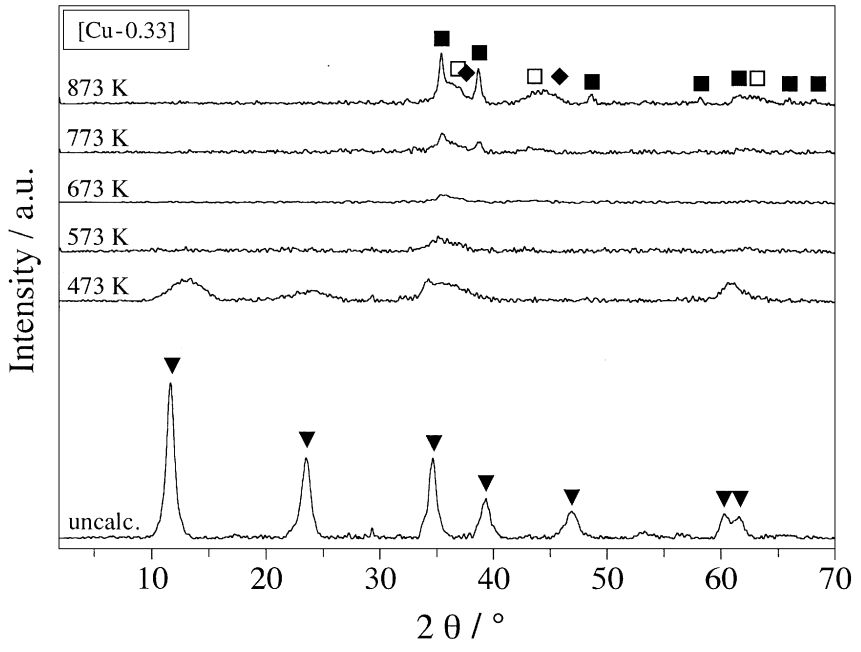

FIG. 4. Crystalline phases of [Cu-0.33] after calcination at different temperatures determined by XRD. (▼) Hydrotalcite-like phase (HT-phase); (■) CuO; (□) MgO; (◆) $CuAl_2O_4$.

Surface areas, pore volumes, and mean pore diameters of [Cu-0.33] were hardly affected by calcination at different temperatures (Table 5). All isotherms were of type-IV with a type-H3 hysteresis according to IUPAC (33), which is generally observed for mesoporous aggregates of platelike particles. Because the samples exhibited similar morphology, intraparticle mass transfer was not expected to be controlling, as shown for $[Cu\text{-}0.33]_{673}$.

Gases evolved during thermal decomposition of [Cu-0.33] were monitored by MS (Fig. 3). TG/DTA data (not shown) as well as evolution of CO_2 and H_2O are characteristic for LDHs (34). An exception was a CO_2 peak in the decomposition pattern around 870 K, which to our knowledge has not been reported so far. CO_2 evolution at this remarkably high temperature was observed in all samples containing crystalline HT.

Morphological changes induced by calcination were studied by TEM (Fig. 5). All samples showed a laminar structure, typical for LDHs (11). Laminae of $[Cu\text{-}0.33]_{uc}$ and $[Cu\text{-}0.33]_{673}$ were smooth, while laminae of $[Cu\text{-}0.33]_{873}$ were covered with little holes (white dots in Fig. 5c) (34). In addition to this lamellar structure, $[Cu\text{-}0.33]_{673}$ and especially $[Cu\text{-}0.33]_{873}$ contained small, spherical particles (black spots in Figs. 5b and 5c).

Cu surface areas of samples calcined at different calcination temperature were determined by N_2O titration and corroborated by XPS (Table 4). Up to 773 K, Cu surface area generally increased with increasing calcination temperature; $[Cu\text{-}0.33]_{873}$ exhibited a slightly lower Cu surface area than $[Cu\text{-}0.33]_{773}$.

TABLE 5

Morphological Properties of [Cu-0.33] Calcined at Different Temperatures Determined by N_2 Physisorption and XRD

Calcination temperature (K)	S_{BET}[a] ($m^2\ g^{-1}$)	V_{p,N_2}[b] ($cm^3\ g^{-1}$)	$d_{p,max}$ ($\langle d_p \rangle$)[c] (nm)	Crystallite size[d] HT (nm)	Crystallite size[d] CuO (nm)
Uncalcined	60	0.50	30 (33)	10	—
473	66	0.47	30 (29)	—	—
573	68	0.50	30 (29)	—	—
673	72	0.52	40 (29)	—	3
773	66	0.56	30 (34)	—	15
873	69	0.48	20 (28)	—	20

[a] BET surface area.
[b] BJH cumulative desorption pore volume.
[c] Graphically assessed maximum of pore size distribution (in parentheses: mean pore diameter, $\langle d_p \rangle = 4V_{p,N_2}/S_{BET}$).
[d] Determined from XRD line broadening.

DISCUSSION

Characteristic Features of Phenylethyne Coupling Reaction

Reaction conditions in the heterogeneous coupling of phenylethyne were chosen so as to eliminate the impact of mass transfer on reaction rate. Hence, the experimental results reflect the behavior of the catalytic system in the kinetically controlled regime.

In analogy to the homogeneous catalytic route (35), the heterogeneous coupling of phenylethyne is believed

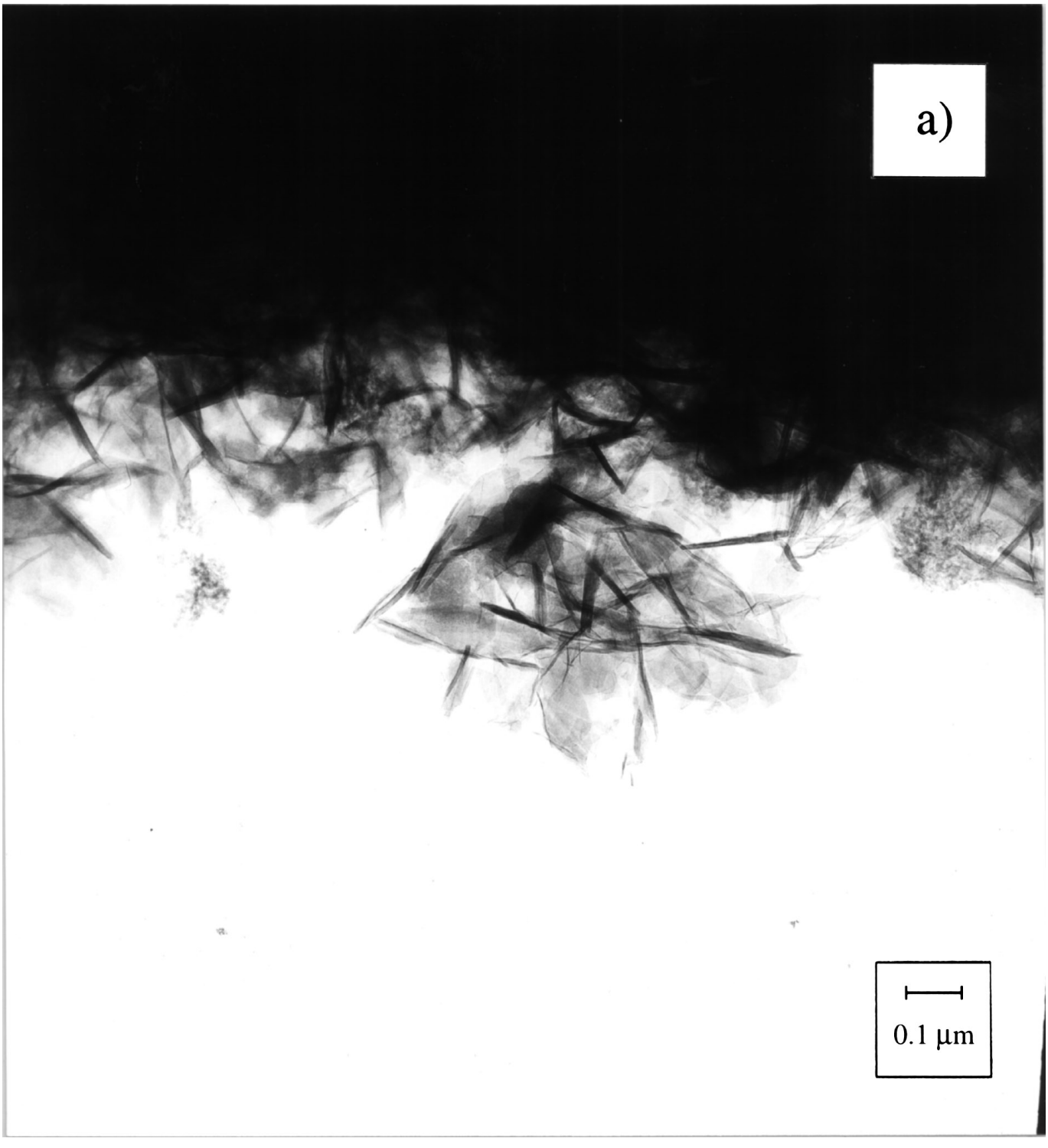

FIG. 5. Morphological changes occurring during calcination as seen by TEM. (a) $[Cu\text{-}0.33]_{uc}$; (b) $[Cu\text{-}0.33]_{673}$; (c) $[Cu\text{-}0.33]_{873}$.

to proceed in three main steps, namely deprotonation of phenylethyne, oxidation of phenylethynilide, and coupling to 1,4-diphenylbuta-1,3-diyne (17). As to the deprotonation of phenylethyne, the intrinsic basicity of the Cu–Mg–Al mixed oxides does not suffice to catalyze this step since no conversion was observed without addition of NaOH to the system. This is possibly due to blocking of the basic sites of the mixed oxides by CO_2 or H_2O (36). The knowledge of the kinetics of the homogeneously catalyzed coupling (37) and the linear dependence of the reaction rate on the amount

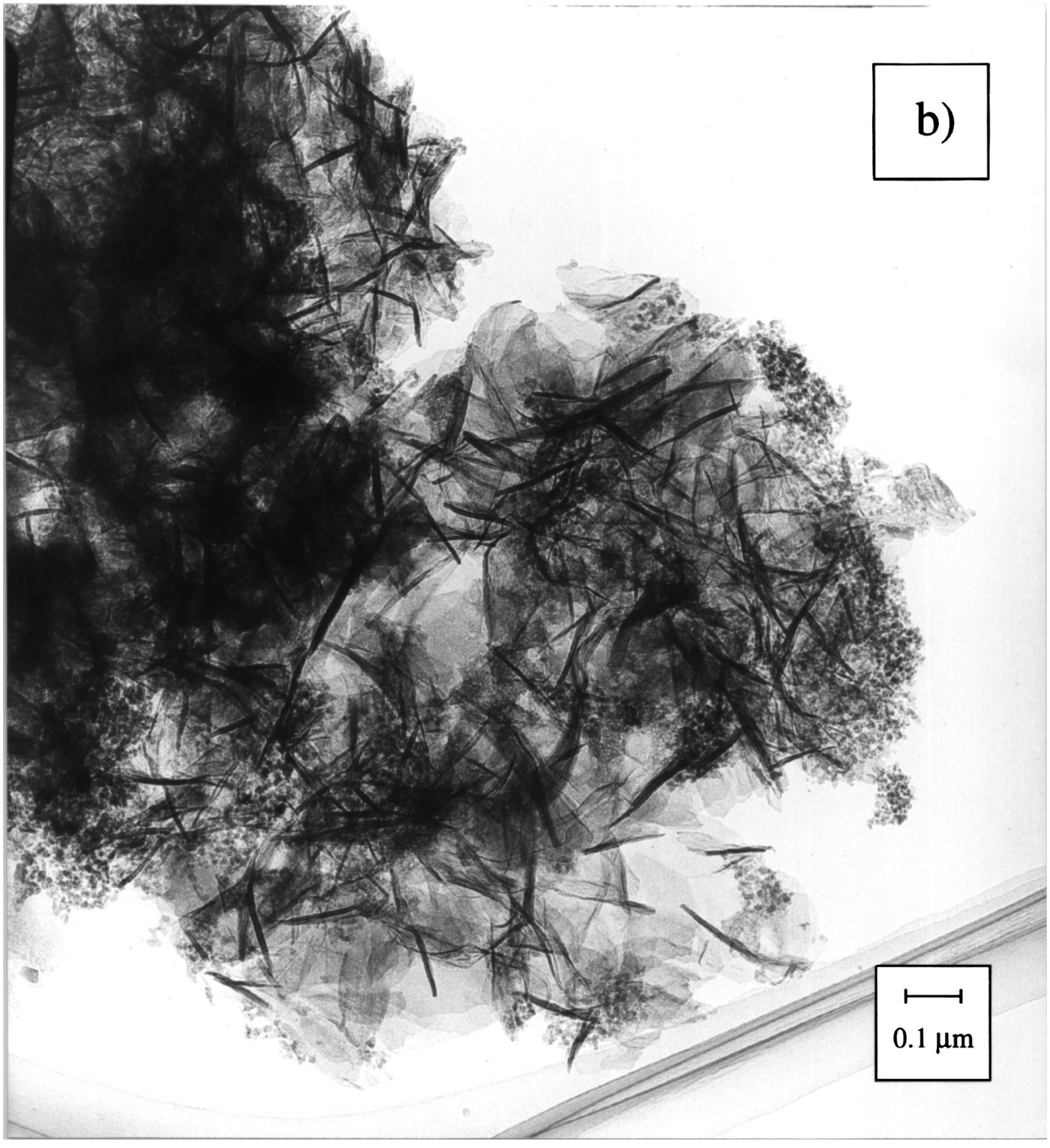

FIG. 5—*Continued*

of catalyst (38) strongly suggest that the deprotonation of phenylethyne is not the rate-limiting step of the reaction, but occurs in a preceding equilibrium. The subsequent step, the oxidation of phenylethynilide is believed to be catalyzed by Cu(II) on the catalyst surface (17). Cu(I) formed in this reaction is reoxidized by oxygen closing the catalytic cycle. Again, this is consistent with studies of the homogeneous coupling route (35, 37). Coupling to 1,4-diphenylbuta-1,3-diyne occurs by combination of two phenylethynilide radicals. Whether the first and third reaction step occur

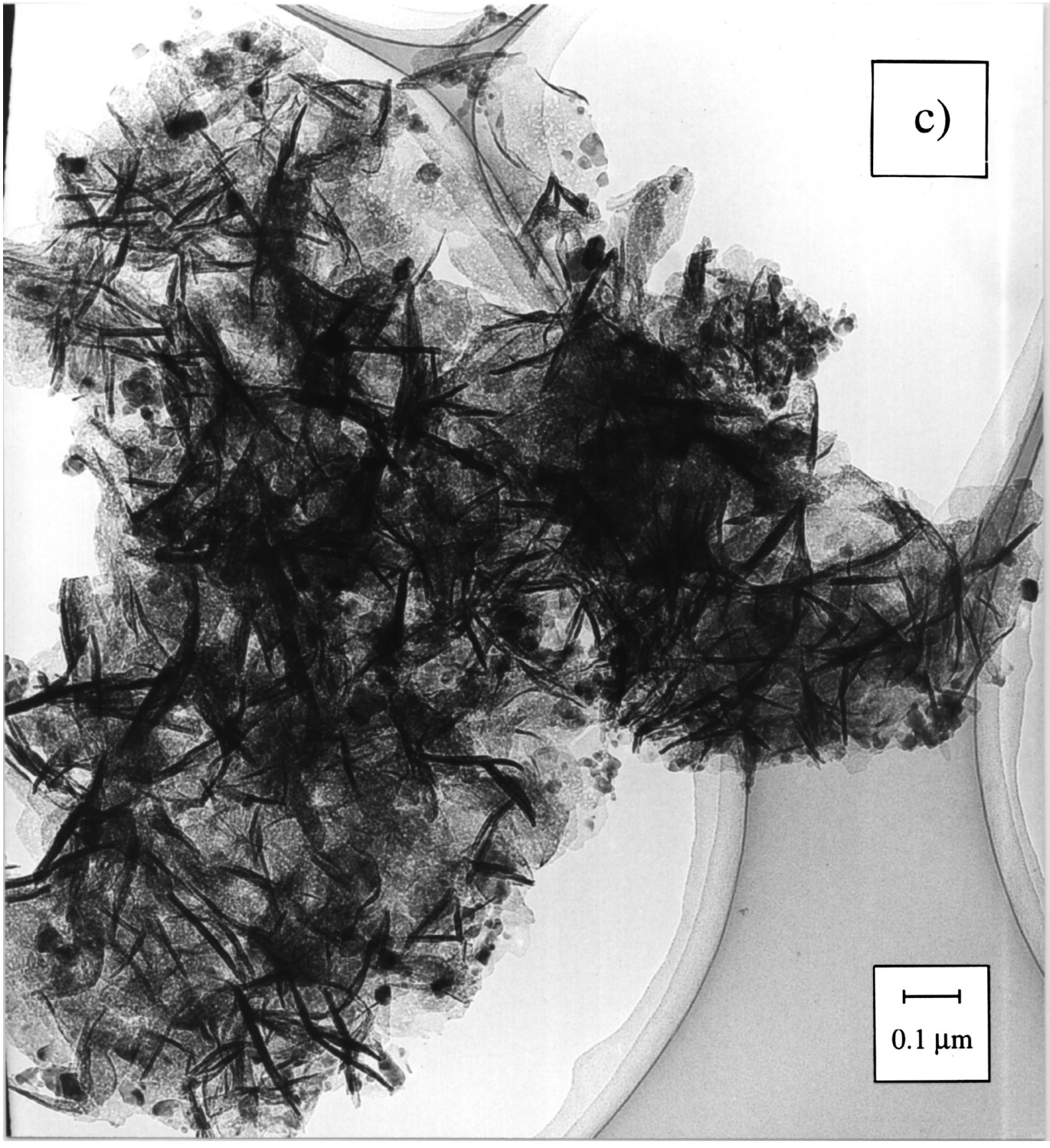

FIG. 5—*Continued*

homogeneously or on the catalyst surface could not be resolved in this study.

Our experimental findings indicate that neither mass transfer nor deprotonation of phenylethyne determines the global reaction rate under the conditions investigated. It seems most likely that the surface reaction involving Cu(II) is the rate-determining step, although this has not been directly proven.

Catalyst Properties

In the subsequent discussion, we assume that the surface reaction involving Cu(II) is rate determining. The kinetic studies indicate that the various Cu–Mg–Al mixed oxides show major differences in activity, whereas the selectivity to 1,4-diphenylbuta-1,3-diyne is only weakly affected by composition (Table 3) and calcination temperature (Table 4). Different activities can originate either from a change in the number of accessible active Cu(II) sites and/or their intrinsic activity.

As to the number of active sites, neither for catalysts with different composition (Table 3) nor for catalyst [Cu-0.33] calcined at different temperatures (Table 4) the *ex situ* measured Cu surface areas can be correlated with conversion of phenylethyne. This is true for Cu surface areas measured both before and after reaction. Although the number of active Cu(II) sites under reaction conditions cannot be safely derived from the measured Cu surface areas, this cannot explain the drastically different catalytic behavior. The fact that $[Cu\text{-}0.0]_{673}$ is not active at all supports this suggestion. Similar behavior has been reported for other reactions involving a Cu species as active site, e.g., methanol synthesis over $Cu–ZnO–Al_2O_3$ (39, 40).

Consequently, the catalysts must differ in the intrinsic activity of the Cu(II) sites. Changes in the redox activity of Cu(II) originate from alterations of the matrix in which Cu(II) is embedded. Catalysts with compositions $[Cu\text{-}0.33]_{673}$, $[Cu\text{-}0.67]_{673}$, $[Cu\text{-}0.29]_{673}$, and $[Cu\text{-}0.25]_{673}$ apparently provide a suitable matrix for active Cu(II), whereas $[Cu\text{-}0.0]_{673}$ does not. For [Cu-0.33], calcined at different temperatures, an activating matrix exists up to temperatures of 773 K, whereas $[Cu\text{-}0.33]_{873}$ exhibits a significant drop in activity indicating major changes in the matrix.

A molecular view on these changes could not be gained in this study. However, our data indicate that the catalysts contained active and inactive phases in varying ratios. For catalysts with different composition, the MgCu-phase in $[Cu\text{-}0.0]_{uc}$ leads to a completely inactive matrix for the Cu(II) catalyzed coupling of phenylethyne, whereas the HT-phase in $[Cu\text{-}0.33]_{uc}$ provides an active matrix (Fig. 2, Table 3). XRD patterns (Fig. 2) and thermal decomposition curves (Fig. 3) of the uncalcined catalysts show that $[Cu\text{-}0.25]_{uc}$ and $[Cu\text{-}0.29]_{uc}$ contained the MgCu-phase and HT-phase in varying ratios, leading to catalysts with medium activity compared to $[Cu\text{-}0.0]_{uc}$ and $[Cu\text{-}0.33]_{uc}$. In fact, the HT portion of the catalysts correlates with the activity of the calcined samples in the coupling reaction. In $[Cu\text{-}0.67]_{uc}$, traces of the HT-phase, providing an active matrix, could be detected by both XRD and thermal decomposition. As concerns [Cu-0.33], calcined at different temperatures, the HT-phase leads to an activating matrix up to temperatures of 773 K. After calcination at 873 K, a major change in the matrix could be detected (Figs. 4 and 5) causing the significant loss in activity for $[Cu\text{-}0.33]_{873}$. This change is related to the evolution of CO_2 at about 870 K (Fig. 3) leading to small holes in the lamellae and spherical particles of CuO (Fig. 5).

In conclusion we can state that the activity of all samples is correlated to the portion of HT in the catalyst, as long as the phase resulting upon calcination is not strongly altered, e.g., by temperatures exceeding 773 K. The HT-phase provides a suitable matrix for active Cu(II). As expected, the effect of this matrix on catalyst activity is more pronounced with well-dispersed Cu(II) than with aggregated Cu(II), where the active sites are partly detached from the matrix.

Studies of the redox behavior of Cu(II) species embedded in the different oxidic matrices will be necessary to gain further insight into the functioning of this complex catalytic system.

CONCLUSIONS

Cu–Mg–Al mixed oxides containing 33 at.% Cu related to the total metal amount prepared by precipitation of metal nitrates with sodium carbonate are efficient catalysts for the oxidative coupling of phenylethyne to 1,4-diphenylbuta-1,3-diyne in the presence of NaOH as cocatalyst. Highest yields of 1,4-diphenylbuta-1,3-diyne (84%) were obtained with catalysts containing a hydrotalcite-like phase.

The heterogeneous coupling of phenylethyne is suggested to proceed in three chemical reaction steps, namely deprotonation of phenylethyne, oxidation of phenylethynilide involving Cu(II) on the catalyst surface, and coupling to 1,4-diphenylbuta-1,3-diyne. The activity of the crucial Cu(II) sites is strongly influenced by the structural and chemical properties of the matrix in which they are embedded. The hydrotalcite-like phase in Cu–Mg–Al catalysts forms a favorable matrix for Cu(II) sites, whereas other phases such as magnesium–copper hydroxide nitrate are less suitable.

ACKNOWLEDGMENTS

Thanks are due to M. Maciejewski for performing thermoanalytical analyses and to R. Wessiken for taking TEM pictures. Financial support by the Swiss National Fonds (Project No. 21-41850.94) is gratefully acknowledged. S.M.A. thanks the Fonds der Chemischen Industrie, Germany, for granting a stipendium.

REFERENCES

1. Cavani, F., Trifirò, F., and Vaccari, A., *Catal. Today* **11**, 173 (1991).
2. Vaccari, A. (Ed.), *Appl. Clay Sci.* **10**, 1 (1995).
3. Reichle, W. T., *Chemtech* 58 (1986).
4. Reichle, W. T., *Solid State Ionics* **22**, 135 (1986).
5. Feitknecht, W., *Helv. Chim. Acta* **25**, 555 (1942).
6. Feitknecht, W., *Helv. Chim. Acta* **25**, 131 (1942).
7. Putyera, K., Bandosz, T. J., Jagiello, J. and Schwarz, J. A., *Appl. Clay Sci.* **10**, 177 (1995).
8. Kooli, F., Kosuge, K., and Tsunashima, A., *J. Solid State Chem.* **118**, 285 (1995).

9. Kannan, S., and Swamy, C. S., *Appl. Catal. B* **3**, 109 (1994).
10. Morpurgo, S., Lo Jacono, M., and Porta, P., *J. Mater. Chem.* **4**, 197 (1994).
11. De Roy, A. D., Forano, C., El Malki, K., and Besse, J. P., *in* "Synthesis of Microporous Materials" (M. L. Occelli and H. E. Robson, Eds.), p. 108. Van Nostrand Reinhold, New York, 1992.
12. Nakatsuka, T., Kawasaki, H., Yamashita, S., and Kohjiya, S., *Bull. Chem. Soc. Jpn.* **52**, 2449 (1979).
13. Kohjiya, S., Sato, T., Nakayama, T., and Yamashita, S., *Macromol. Chem. Rapid Commun.* **2**, 231 (1981).
14. Reichle, W. T., *J. Catal.* **94**, 547 (1985).
15. Busetto, C., Del Piero, D., Manara, G., Trifirò, F., and Vaccari, A., *J. Catal.* **85**, 260 (1984).
16. Kaneda, K., Ueno, S., and Imanaka, T., *J. Chem. Soc., Chem. Commun.* 797 (1994).
17. Auer, S. M., Schneider, M., and Baiker, A., *J. Chem. Soc., Chem. Commun.* 2057 (1995).
18. Khoo, I.C., and Wu, S. T., *in* "Optics and Nonlinear Optics of Liquid Crystals," p. 42. World Scientific, Singapore, 1993.
19. Hay, A. S., *J. Org. Chem.* **27**, 3320 (1962).
20. Sonogashira, K., *in* "Comprehensive Organic Synthesis" (B. M. Trost and I. Fleming, Eds.), p. 551. Pergamon Press, Oxford, 1991.
21. "Mineral Powder Diffraction Data Files." JCPDS-International Center for Diffraction Data, Swarthmore, PA, 1995.
22. Scherrer, P., *Gött. Nachr.* **2**, 98 (1918).
23. Klug, H. P., and Alexander, L. E., "X-Ray Diffraction Procedures for Polycrystalline and Amorphous Materials." Wiley, New York, 1974.
24. Halder, N. C., and Wagner, C. N. J., *Acta Cryst.* **20**, 312 (1966).
25. Pause, H., and Mensing, J., "SpecsLab 1.6." Specs GmbH, Berlin, 1996.
26. Briggs, D., and Seah, M. P., "Practical Surface Analysis by Auger and X-Ray Photoelectron Spectroscopy." Wiley, Chichester, 1983.
27. Evans, J. W., Wainwright, M. S., Bridgewater, A. J., and Young, D. J., *Appl. Catal.* **7**, 75 (1983).
28. Chinchen G. C., Hay, C. M., Vanderwell, H. D., and Waugh, K. C., *J. Catal.* **103**, 79 (1987).
29. Barrett, E. P., Joyner, L. G., and Halenda, P. P., *J. Am. Chem. Soc.* **73**, 373 (1951).
30. Broekhoff, J. C. P., *in* "Preparation of Heterogeneous Catalysts II" (P. G. B. Delmon, P. Jakobs, and G. Poncelet, Eds.), Vol. 3, p. 663. Elsevier, Amsterdam, 1979.
31. Harkins, W. D., and Jura, G., *J. Chem. Phys.* **11**, 431 (1943).
32. "Gmelin Handbook of Inorganic Chemistry, Copper Organic Compounds, Part 3." Springer Verlag, Berlin, 1986.
33. Sing, K. S. W., *et al.*, *Pure Appl. Chem.* **57**, 603 (1985).
34. Reichle, W. T., Kang, S. Y., and Everhardt, D. S., *J. Catal.* **101**, 352 (1986).
35. Klebansky, A. L., Grachev, I. V., and Kuznetsova, O. M., *Zh. Obshch. Khim.* **27**, 2977 (1957).
36. Tanabe, K., *in* "Catalysis by Acids and Bases" (B. Imelik, C. Naccache, G. Coudurier, Y. Ben Taarit, and J. C. Vedrine, Eds.), Vol. 20, p. 1. Elsevier, Amsterdam, 1985.
37. Bohlmann, F., Schönowsky, H., Inhoffen, E., and Grau, G., *Chem. Ber.* **97**, 794 (1964).
38. Auer, S. M., Wandeler, R., Schneider, M., and Baiker, A., *in* "Proceedings, Catalysis on Solid Acids and Bases" (J. Weitkamp and B. Lücke, Eds.), 9601, p. 23. DGMK German Society for Petroleum and Coal Science and Technology, Berlin, 1996.
39. Gusi, S., Trifirò, F., Vaccari, A., and Del Piero, G., *J. Catal.* **94**, 120 (1985).
40. Doesburg, E. B. M., Höppener, R. H., de Koning, B., Xiaoding, X., and Scholten, J. J. F., *in* "Preparation of Catalysts IV" (B. Delmon, P. Grange, P. A. Jacobs, and G. Poncelet, Eds.), p. 767. Elsevier, Amsterdam, 1987.